Phase Separation in Wetting Ridges of Sliding Drops on Soft and Swollen Surfaces

Lukas Hauer,[1,2,*] Zhuoyun Cai,[2,*] Artem Skabeev,[3] Doris Vollmer,[1,†] and Jonathan T. Pham[2,‡,∥]
[1]Max Planck Institute for Polymer Research, Ackermannweg 10, 55128 Mainz, Germany
[2]Department of Chemical and Materials Engineering, University of Kentucky, Lexington, 40506 Kentucky, USA
[3]Institute of Organic Chemistry and Macromolecular Chemistry, Friedrich Schiller University Jena, Lessingstrasse 8, 07743 Jena, Germany

(Received 12 August 2022; accepted 11 January 2023; published 3 February 2023)

Drops in contact with swollen, elastomeric substrates can induce a capillary mediated phase separation in wetting ridges. Using confocal microscopy, we visualize phase separation of oligomeric silicone oil from a cross-linked silicone network during steady-state sliding of water drops. We find an inverse relationship between the oil tip height and the drop sliding speed, which is rationalized by competing transport timescales of the oil molecules: separation rate versus drop-advection speed. Separation rates in highly swollen networks are as fast as diffusion in pure melts.

DOI: 10.1103/PhysRevLett.130.058205

Classically, wetting is characterized by the Young-Dupré contact angle at the three-phase-contact line of a drop on a substrate [1]. However, when the underlying substrate is a liquid or a soft solid, this angle does not suffice because of an out-of-plane ridge formation [2–4]. A "wetting ridge" emerges due to the drop surface tension, which pulls on the substrate and deforms it upwards [5–14]. On pure liquid substrates, the ridge geometry is solely governed by capillarity, while on soft solid substrates, elastic contributions add to the ridge geometry [15–17]. The Neumann angles consider force balances not only in the horizontal but also in the vertical direction [18], and can help recover a better description of the wetting situation [19–21].

Although wetting of pure liquid or soft solid substrates are typically treated as two distinct cases, many soft substrates have features of both [22–26]. For example, cross-linked polymeric substrates are often swollen with unbound, free molecules (e.g., oligomers in elastomers or water in hydrogels); this leads to a complex combination of liquid and solid behaviors. Recently, it has been shown that ridges on swollen, lightly cross-linked elastomers do not necessarily comprise a homogeneous phase. Unbound molecules phase separate at the tip of the ridge, forming a region of pure liquid [27–29]. However, these have been mostly considered in static drops.

In dynamic wetting conditions, the ridge is highly relevant: Friction that builds up during drop sliding dissipates mostly in the ridge [30–33]. Hence, the shape and material makeup of the wetting ridge are central components to determine drop movement. For soft, swollen elastomers, the presence of free molecules is likely to alter the drop dynamics [34–37]. Yet, it is not well understood how drop sliding speed couples to phase separation, how sliding-induced separation is related to the swelling ratio of the underlying network, and what timescales govern the separation mechanism.

In this Letter, we investigate wetting ridges on soft polydimethylsiloxane (PDMS) substrates, swollen with silicone oil (liquid oligomers), during steady-state sliding of water drops. The network and oil are dyed with individual fluorescence markers, enabling independent visualization of each phase by laser scanning confocal microscopy (LSCM). Cross-sectional views of the moving wetting ridge yield their shape and the spatial distribution of network and oil phases in the ridge. For highly swollen networks, the extent of phase separation depends on the sliding speed of the drop, which is suppressed at fast sliding speeds. However, no phase separation is observed on less swollen substrates, even for slower moving drops. From images of the speed-dependent wetting ridge, we extract the mobility of phase separating oil that approaches values of free melt diffusion (up to 0.4 $\mu m^2/ms$).

Material system.—Soft PDMS networks (Young's modulus $E \approx 3$–5 kPa) with different amounts of swelling agent (i.e., ratio of swollen to dry network volume $Q = V_{swollen}/V_{dry}$) were manufactured and placed on glass slides (synthesis, rheology, and pore pressure Π given in Supplemental Material [38], and Ref. [39]). Q ranges from 7.5 ($\Pi \approx 16.5$ kPa) to 16 ($\Pi \approx 3.4$ kPa), i.e., nearly saturated. PDMS networks were initially cleaned of uncross-linked material followed by reswelling with silicone oil having well-defined low molecular weight (770 g/mol, Gelest). The substrate thickness is ≈100 μm, sufficiently

large to not interfere with the wetting ridge while still allowing for clear confocal imaging [49].

Phase-separated wetting ridge of dynamic drops.—The swollen PDMS networks are mounted on a motorized linear stage over a confocal microscope (Leica SP8). An 8 μl water drop (large enough to neglect evaporation but small enough to facilitate easy sliding) is then placed on the substrate. Upon deposition, there is an initial dwell time, in which an annular wetting ridge forms at the three-phase contact line. A metal ring (diameter ≈2.5 mm) is fixed 1 mm above the substrate and holds the drop in position while the stage moves at constant speeds ($5 - 800$ μm/s), Fig. 1(a). This generates a relative sliding motion between the drop and substrate, while the drop remains fixed in the laboratory frame for imaging. The drop is positioned such that the advancing contact zone lies in the confocal field of view, which spans 250×62 μm^2. While the drop is brought up to its set-point speed, the system shows transient start-up dynamics; however, this regime of motion lies outside the scope of our current study on steady-state dynamics. In steady state, the wetting ridge assumes a near-constant shape at a stationary position within the field of view, even during long sliding times (> 200 s). We note that the wetting ridge shape does not depend on the dwell time of the drop prior to sliding. On rare occasions, the ridge deviates from its stationary position due to contact line pinning, likely stemming from surface impurities or contamination [50–52]. Images are taken 1.6 times/ sec, which enables resolving these motions. This fast recording, however, brings higher signal noise with it—a drawback that we overcome by aligning each image by the tip of the ridge, followed by averaging, Supplemental Material [38].

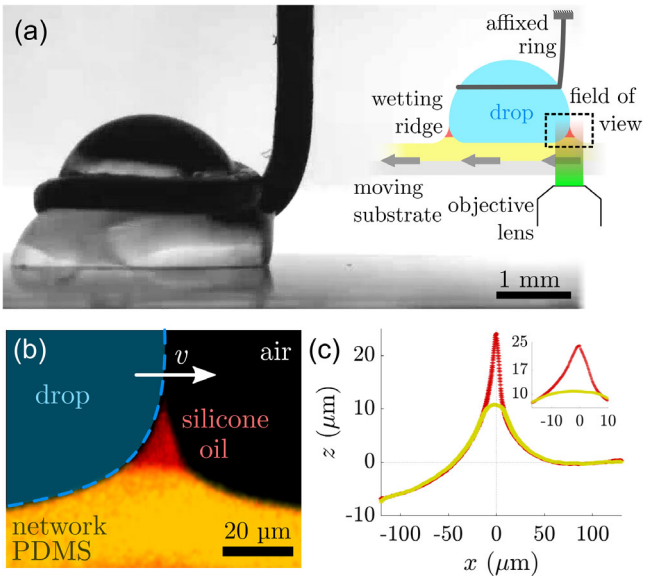

FIG. 1. Drop sliding setup and wetting ridge visualization. (a) Macroscopic side view of affixed drop, sliding at 5 μm/s on a swollen PDMS network ($Q = 14.5$). Substrate moves left while drop is stationary. Inset, setup schematic. (b) Temporal averaged ($n = 158$) LSCM image of a phase-separated wetting ridge. PDMS network and silicone oil are dyed separately with fluorescence markers with different emission spectra. Red shows silicone oil and orange shows swollen PDMS network. (c) Extracted interfaces of silicone oil (red points) and PDMS network (yellow points). Inset, blown-up section of the phase-separated zone in the wetting ridge. Standard errors are smaller than the symbol size.

To illustrate the core features of the moving, phase-separated wetting ridge, we first slide drops over a swollen substrate ($Q = 14.5$) at a speed of 5 μm/s. We start recording images 20–30 s after the onset of sliding, when no more variations are observed in the ridge shape. The dynamic wetting ridge is recorded for ≈250 s. This gives $n = 158$ images that yield a crisp reconstruction of the averaged wetting zone, Fig. 1(b). The wetting ridge clearly shows two phases of (i) swollen, network PDMS (orange) and (ii) pure liquid silicone oil (red). While the network height is only slightly elevated, the silicone oil forms a sharp tip. Extracting the interfaces of each phase reveals more quantifiable detail, Fig. 1(c). The small relative errors of the temporally accumulated data indicate that indeed, the ridge is in a steady state. At $x = 0$, the wetting ridge has its highest point. At $|x| \gg 0$, interfacial profiles of the two phases (red and yellow) align. At $x \ll 0$, the PDMS network profile is dented due to the Laplace pressure in the drop acting on the substrate. The network and the silicone oil are well separated between -15 μm $\lesssim x \lesssim 8$ μm, Fig. 1(c) inset. Within this range, the ridge profile is asymmetric with more silicone oil towards the drop ($x < 0$). Additionally, in the separated region, the network profile bends into the oil phase. The positive curvature of the network profile indicates an overpressure inside the network PDMS with respect to the oil phase. At $x = 0$, phase separation is strongest with a separation height of more than 10 μm.

Sliding speed and swelling ratio variation.—Next, we vary the sliding speed ($v = 5$–800 μm/s) and the substrate swelling ratio ($Q = 7.5$–16, near saturation). The ridge profiles of silicone oil are shown in Fig. 2(a) for $Q = 16$ at various sliding speeds, together with the network profiles in the inset. The corresponding averaged LSCM images at the slow and fast speeds are shown in the top row. The highest ridge (≈35 μm) forms at low sliding speed (5 μm/s, dark blue). Increasing v gradually decreases the ridge height. The smallest recorded ridge is less than 20 μm at $v =$ 800 μm/s (light yellow). This height-speed relationship is inverted for the network profile, i.e., the network rises with increasing speed. However, the sensitivity of the network height to v is not as pronounced as for the silicone oil tip height, Fig. 2(b). With increasing speed, the decrease in maximum oil height $h_{\mathrm{oil,max}}$ (red circles) is much steeper than the increase in maximum network height $h_{\mathrm{net,max}}$ (yellow circles). For $v > 100$ μm/s, the height difference between $h_{\mathrm{oil,max}}$ and $h_{\mathrm{net,max}}$ is only 1–3 μm. For substrates swollen to a lesser extent ($Q = 14.5$), we observe smaller

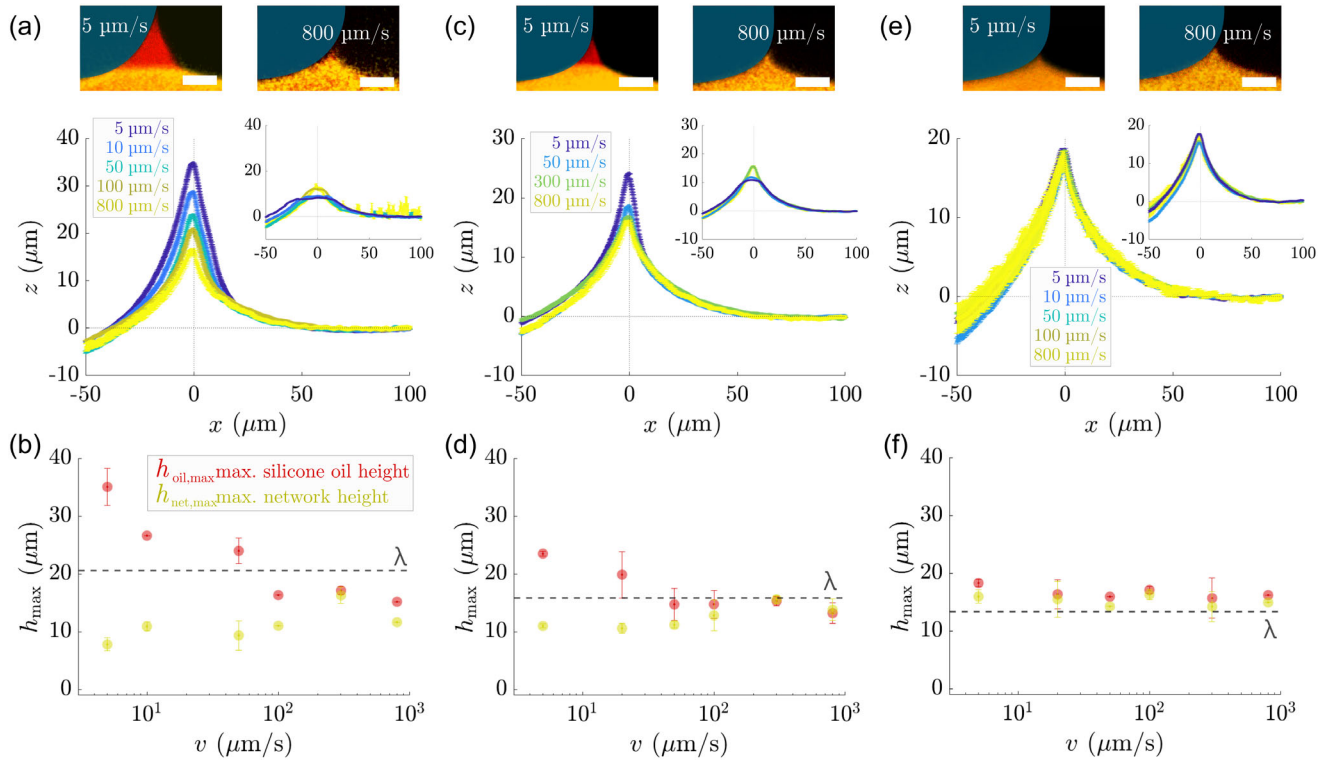

FIG. 2. Dynamic wetting ridge shape for different sliding speeds and swelling ratios (a),(b) $Q = 16$, (c),(d) $Q = 14.5$, (e),(f) $Q = 10$. (a),(c),(e) Dynamic ridge profiles of liquid silicone oil (and network PDMS as insets). (a),(c) For silicone oil, the ridge height gradually decreases for increasing drop speed, $v = 5$, 10, 50, 100, 300, 800 μm/s. Top row images are representative LSCM images for $v = 5$ and $v = 800$ μm/s (scale bar 20 μm). (b),(d),(f) Maximum height of dynamic ridges of silicone oil (red) and network PDMS (yellow). Data shows average of min. $n = 3$ repetitions together with standard deviations. Dashed lines mark dynamic elastocapillary height $\lambda \sim \gamma \sin\theta_{\mathrm{adv}}/E$, which are (b) 21 μm ($E \approx 3$ kPa) (d) 16 μm ($E \approx 3.9$ kPa), (f) 13 μm ($E \approx 4.8$ kPa).

ridge heights (≈25 μm for $v = 5$ μm/s) and narrower widths compared to the saturated ($Q = 16$) substrate, Figs. 2(c)–2(d). The less swollen substrate also has a less sensitive height-speed dependency. For $v > 100$ μm/s, the silicone oil does not clearly separate. When substrates are swollen even less to $Q = 10$, phase separation is not visible in our images; within experimental accuracy, all ridges collapse to the same shape, independent of sliding speed, i.e., $h_{\mathrm{oil,max}} \approx h_{\mathrm{net,max}}$, Fig. 2(e). The maximum ridge height reaches about 15 μm for all speeds tested. These results illustrate that sliding speed and swelling ratio are critical factors that govern phase separation in dynamic wetting. To obtain a mechanical picture of the (separated) ridge, we now relate the network height to the acting force. The network PDMS is (visco)elastic and adapts its shape to imposed stresses. Therefore, $h_{\mathrm{net,max}}$ is a proxy for the force f, acting on the material [53] per

$$h_{\mathrm{net,max}} \sim f/E, \tag{1}$$

where E is the Young's modulus of the swollen network [29]. In cases without phase separation, the force is imposed at a singular point by the capillary action of the drop,

$$f \sim \gamma \sin\theta_{\mathrm{adv}}, \tag{2}$$

where γ is the drop surface tension and θ_{adv} the advancing contact angle. Hence, $h_{\mathrm{net,max}}$ should coincide with the advancing elastocapillary length

$$\lambda \sim \gamma \sin\theta_{\mathrm{adv}}/E. \tag{3}$$

Swollen PDMS has an advancing contact angle of $\theta_{\mathrm{adv}} \approx 105°$ [54]. Liquid silicone oil tends to cloak aqueous drops and consequently lowers γ from 72 to 64 mN/m [55,56]. When no phase separation is detected, λ and $h_{\mathrm{net,max}}$ coincide within experimental margin, Figs. 2(b), 2(d), and 2(f), dashed line. Discrepancies may arise from small measurement errors of E and from the omission of the geometrical prefactors [57]. For substrates of $Q > 10$, the transition to suppressed phase separation happens at speeds around $v > 100$ μm/s. On $Q \leq 10$, $h_{\mathrm{oil,max}} \approx h_{\mathrm{net,max}}$ for all v, indicating that phase separation is mostly suppressed—although a very thin layer that is not visible likely exists. For $Q = 16$ and 14.5, $h_{\mathrm{net,max}}$ decreases with decreasing speeds. The height-speed trend inverses for $h_{\mathrm{oil,max}}$. This indicates a coupling between $h_{\mathrm{oil,max}}$ and $h_{\mathrm{net,max}}$: In cases of phase separation, the normal force acting on the network relaxes from the initial capillary-induced force, Eq. (2), over the region of phase separation. Alternatively, $h_{\mathrm{net,max}}$ may also change due to altered material composition

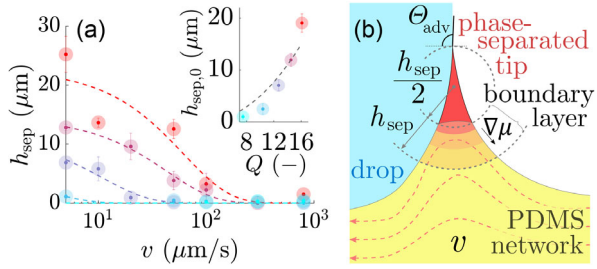

FIG. 3. Separation of liquid, silicone oil. (a) Separation height h_{sep} versus v, for $Q = 16$ (cherry red), $Q = 14.5$ (bordeaux), $Q = 12.7$ (dark blue), $Q = 10$ (blue), and $Q = 7.5$ (turquoise). Dashed lines show exponential relaxation per Eq. (6). Inset, measured $h_{sep,0}$ at zero speed for different Q. The dashed line shows $h_{sep,0}$, when the balance Eq. (4) is met. (b) Competing transport mechanisms of phase separating, silicone oil molecules induced by $\nabla\mu$ and sliding speed v. The boundary layer where $\nabla\mu \neq 0$ penetrates $\approx h_{sep}/2$ into the network bulk.

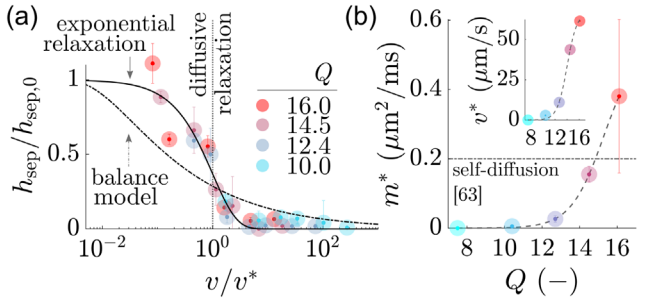

FIG. 4. Separation dynamics and mobilities. (a) Normalized tip height $h_{sep}/h_{sep,0}$ against normalized sliding speed v/v^* (colored circles). Dashed line: balance model; and solid line: exponential relaxation. (b) Measured mobility m^* against Q. Horizontal line is the mobility of self-diffusion [63]. Inset shows extracted correlation speed v^*. Dashed lines indicate trends and error bars correspond to fitted root-square-mean error.

(i.e., E) in the network ridge when phases separate. However, we expect that the material composition in the network remains largely unaffected by variations in v, due to the large reservoir of silicone oil in the bulk.

Dynamic separation height.—The size of the separated liquid tip $h_{sep} = h_{oil,max} - h_{net,max}$ ranges between $h_{sep,0}$ at $v = 0$ down to 0 for $v \to \infty$, Fig. 3(a). The initial separation height becomes visible for $Q > 8$ and becomes more pronounced for larger Q, Fig. 3(a) inset. Physically, the separation is driven by differing chemical potentials in the tip μ_{tip} and in the bulk network μ_{net}. As the tip is purely liquid, μ_{tip} is governed by the internal tip pressure. The liquid tip pressure changes with the interfacial curvature (Laplace pressure), and thus, also changes with h_{sep}. μ_{net} depends on the pore pressure, and therefore on Q. The dashed line in the inset of Fig. 3(a) shows $h_{sep,0}$, solely balanced by the pore pressure, which shows reasonable overlay to the data at zero speed, Supplemental Material [38]. The potential difference invokes the oil flux from the network to the tip, $j_{diff} = -m\nabla\mu$, where m is the flux mobility. Given the poroelastic nature of the flux [58–61], the mobility can be thought of as a Darcy type, $m = k/\eta\Omega^2$, where k is the network permeability, $\eta = 4.6$ mPa s the viscosity, and $\Omega = 840$ mL/mol the molar volume of the low molecular weight silicone oil [62]. The region under the tip, where $\nabla\mu \neq 0$, resembles a diffusive boundary layer, which has a size $\approx h_{sep}/2$, Fig. 3(b). In equilibrium, the tip separates to $h_{sep,0}$ [Fig. 3(a) inset] and the chemical potentials balance

$$\mu_{tip}(h_{sep,0}) = \mu_{net}(Q). \tag{4}$$

$h_{sep,0}$ is reached after a time given by $\tau^* = h_{sep,0}^2/4m$. The equilibrium values τ^* and $h_{sep,0}/2$ allow us to construct an equilibration speed $v^* = h_{sep,0}/2\tau^*$.

When the drop is brought into sliding motion, an advective flux builds up in the reference frame of the ridge, $j_{adv} = \Omega v$, which superposes j_{diff}. This hinders the full static equilibration of the tip as the region underneath the tip is constantly refreshed. At constant sliding motion, however, a steady state exists. This steady-state is only possible when the two fluxes balance,

$$j_{diff} = j_{adv}. \tag{5}$$

Additional fluxes from the cloaking layer or an oil precursor on the network surface may contribute. However, the interfacial area between these fluxes and the tip is smaller than the ones from j_{diff} and j_{adv} by a few orders of magnitude and are therefore comparatively minor; hence, these are neglected in our description. When the sliding speed is sufficiently large, the advective flux can fully suppress separation. We condense the flux balance [Eq. (5)] and the equilibrium condition [Eq. (4)] into a steady-state "balance model" (cf. Supplemental Material [38] for full derivations). The model estimates the speed-dependent separation height; the dashed-dotted line in Fig. 4(a) shows the renormalized model estimate. To compare our data with the balance model, we extract v^* from our data by calculating the correlation speed of the measured $h_{sep}(v)$ using the correlation function $\mathrm{corr}\{h_{sep}, h_{sep,0}\}$, Supplemental Material [38]. We find that the normalized speed-correlation function is well represented by a decaying exponential

$$\mathrm{corr}\{h_{sep}, h_{sep,0}\} \approx h_{sep}(v)/h_{sep,0} \approx e^{-v/v^*}. \tag{6}$$

Renormalization of the height and speed as $h_{sep}/h_{sep,0}$ and v/v^* collapses the data onto the exponential relaxation curve, Fig. 4(a). The balance model recovers the experimentally observed separation (and the exponential relaxation) for $v \to 0$ and $v \to \infty$, Fig. 4(a) dashed-dotted line.

For $v/v^* < 1$, the modeled separation is underestimated while for $v/v^* > 1$ it is slightly overestimated. These deviations may stem from h_{sep}-dependent, elastic contributions to μ_{net} in the boundary layer. Additionally, the omission of geometrical factors may introduce further uncertainties.

The extracted heights and speeds produce an effective mobility $m^* = v^* h_{sep,0}/2$ of the separating oil. Consequently, m^* is only measurable when a tip separates; that is, the mobility is $m^* \approx 0$ for $Q \leq 10$, Fig. 4(b). For $Q > 10$, m^* increases with Q. At high Q, $\mathcal{O}(m^*) = 10^{-10}$ m^2/s, which is close to the mobilities of self-diffusing (low Ω) PDMS molecules in melts [63], Fig. 4(b) horizontal line. The increasing m^* at higher Q can be explained by considering the network structure: When more oil is swollen into the network, the pores of the network (i.e., mesh size) are expanded [64]. When molecules travel through the expanded pores, the imposed friction from the immobilized (cross-linked) network is reduced. This is reflected in higher permeability values k, and hence, a higher Darcy mobility. At a given prevailing chemical potential gradient, combined with an inherent excess in available oil molecules, high swelling ratios lead to faster molecular fluxes, and ultimately, to faster and larger ridge formations. Eventually, the imposed friction in strongly expanded networks stems dominantly from internal molecular friction, since the interactions with the immobile network become negligible. Hence at a high swelling ratio, our data suggest a crossover from a Darcy transport to melt diffusion.

In summary, the competition of drop advection and molecular flux governs the degree of phase separation in wetting ridges of moving drops. Understanding phase separation should offer guidelines for controlling drop dynamics. Notably, phase separation is locally triggered by the (weak) singularity of the three-phase contact line. Whether phase separation occurs spontaneously or requires some threshold effort remains an open and relevant question for wetting on soft substrates.

We thank Rodrique G. M. Badr, Abhinav Naga, Friederike Schmid, and William S. Y. Wong for discussions. This research is supported by the U.S. National Science Foundation through Grant No. 2043732 (Z. C., J. T. P.), the German Research Foundation (DFG) with the Priority Programme 2171 (L. H., D. V.), and the Max Planck Center for Complex Fluid Dynamics—University of Twente (D. V.).

*These authors contributed equally.
†vollmerd@mpip-mainz.mpg.de
‡Jonathan.Pham@uc.edu
‖Present address: Department of Chemical and Environmental Engineering, University of Cincinnati, Cincinnati, OH, USA.

[1] T. Young, Phil. Trans. R. Soc. London **95**, 65 (1805).
[2] S. H. Yuk and M. S. Jhon, J. Colloid Interface Sci. **110**, 252 (1986).
[3] F. Schellenberger, J. Xie, N. Encinas, A. Hardy, M. Klapper, P. Papadopoulos, H.-J. Butt, and D. Vollmer, Soft Matter **11**, 7617 (2015).
[4] C. Semprebon, G. McHale, and H. Kusumaatmaja, Soft Matter **13**, 101 (2016).
[5] A. Carré, J.-C. Gastel, and M. E. R. Shanahan, Nature (London) **379**, 432 (1996).
[6] E. Saiz, A. Tomsia, and R. Cannon, Acta Mater. **46**, 2349 (1998).
[7] C. Clanet and D. Quéré, J. Fluid Mech. **460**, 131 (2002).
[8] F. Léonforte and M. Müller, J. Chem. Phys. **135**, 214703 (2011).
[9] S. J. Park, J. B. Bostwick, V. D. Andrade, and J. H. Je, Soft Matter **13**, 8331 (2017).
[10] J. Gerber, T. Lendenmann, H. Eghlidi, T. M. Schutzius, and D. Poulikakos, Nat. Commun. **10**, 4776 (2019).
[11] R. Masurel, M. Roché, L. Limat, I. Ionescu, and J. Dervaux, Phys. Rev. Lett. **122**, 248004 (2019).
[12] B. Andreotti and J. H. Snoeijer, Annu. Rev. Fluid Mech. **52**, 285 (2020).
[13] Z. Dai and D. Vella, Phys. Rev. Fluids **7**, 054003 (2022).
[14] K. Chaudhuri and J. T. Pham, Soft Matter **18**, 3698 (2022).
[15] S. Mora, T. Phou, J.-M. Fromental, L. M. Pismen, and Y. Pomeau, Phys. Rev. Lett. **105**, 214301 (2010).
[16] E. R. Jerison, Y. Xu, L. A. Wilen, and E. R. Dufresne, Phys. Rev. Lett. **106**, 186103 (2011).
[17] J. Bico, E. Reyssat, and B. Roman, Annu. Rev. Fluid Mech. **50**, 629 (2018).
[18] A. W. Neumann, R. J. Good, C. J. Hope, and M. Sejpal, J. Colloid Interface Sci. **49**, 291 (1974).
[19] A. Marchand, S. Das, J. H. Snoeijer, and B. Andreotti, Phys. Rev. Lett. **109**, 236101 (2012).
[20] Z. Cao and A. V. Dobrynin, Macromolecules **48**, 443 (2015).
[21] M. van Gorcum, S. Karpitschka, B. Andreotti, and J. H. Snoeijer, Soft Matter **16**, 1306 (2020).
[22] T. Tanaka, Sci. Am. **244**, No. 1, 124 (1981).10.1038/scientificamerican0181-124
[23] T. Tanaka, S.-T. Sun, Y. Hirokawa, S. Katayama, J. Kucera, Y. Hirose, and T. Amiya, Nature (London) **325**, 796 (1987).
[24] J. N. Lee, C. Park, and G. M. Whitesides, Anal. Chem. **75**, 6544 (2003).
[25] E. P. Chan and A. J. Crosby, Adv. Mater. **18**, 3238 (2006).
[26] E. P. Chan, E. J. Smith, R. C. Hayward, and A. J. Crosby, Adv. Mater. **20**, 711 (2008).
[27] K. E. Jensen, R. Sarfati, R. W. Style, R. Boltyanskiy, A. Chakrabarti, M. K. Chaudhury, and E. R. Dufresne, Proc. Natl. Acad. Sci. U.S.A. **112**, 14490 (2015).
[28] J. T. Pham, F. Schellenberger, M. Kappl, and H.-J. Butt, Phys. Rev. Mater. **1**, 015602 (2017).
[29] Z. Cai, A. Skabeev, S. Morozova, and J. T. Pham, Commun. Mater. **2**, 21 (2021).
[30] M. E. R. Shanahan and A. Carre, Langmuir **11**, 1396 (1995).
[31] D. Long, A. Ajdari, and L. Leibler, Langmuir **12**, 5221 (1996).
[32] S. Karpitschka, S. Das, M. van Gorcum, H. Perrin, B. Andreotti, and J. H. Snoeijer, Nat. Commun. **6**, 7891 (2015).

[33] M. Zhao, J. Dervaux, T. Narita, F. Lequeux, L. Limat, and M. Roché, Proc. Natl. Acad. Sci. U.S.A. **115**, 1748 (2018).
[34] A. Hourlier-Fargette, A. Antkowiak, A. Chateauminois, and S. Neukirch, Soft Matter **13**, 3484 (2017).
[35] M. Zhao, F. Lequeux, T. Narita, M. Roché, L. Limat, and J. Dervaux, Soft Matter **14**, 61 (2018).
[36] W. S. Y. Wong, L. Hauer, A. Naga, A. Kaltbeitzel, P. Baumli, R. Berger, M. D'Acunzi, D. Vollmer, and H.-J. Butt, Langmuir **36**, 7236 (2020).
[37] Q. Xu, L. A. Wilen, K. E. Jensen, R. W. Style, and E. R. Dufresne, Phys. Rev. Lett. **125**, 238002 (2020).
[38] See Supplemental Material at http://link.aps.org/supplemental/10.1103/PhysRevLett.130.058205 for details on swollen PDMS substrate preparation, which includes Ref. [39]; details for LSCM image processing and source codes; for the pore pressure determination, which includes Refs. [29,40–45]; for detailed model derivations, which includes Refs. [46–48]; and a presentation of speed-correlation function and exponential relaxation.
[39] J. D. Glover, C. E. McLaughlin, M. K. McFarland, and J. T. Pham, J. Polym. Sci. **58**, 343 (2020).
[40] M. L. Huggins, J. Chem. Phys. **9**, 440 (1941).
[41] P. J. Flory, J. Chem. Phys. **9**, 660 (1941).
[42] F. Horkay, A.-M. Hecht, and E. Geissler, J. Polym. Sci. B **33**, 1641 (1995).
[43] S. Venkatraman, A. Nixon, and A. Highe, J. Appl. Polym. Sci. **52**, 1619 (1994).
[44] S. T. Milner, M.-D. Lacasse, and W. W. Graessley, Macromolecules **42**, 876 (2009).
[45] M. Gottlieb and M. Herskowitz, Macromolecules **14**, 1468 (1981).\
[46] D. Daniel, J. V. I. Timonen, R. Li, S. J. Velling, and J. Aizenberg, Nat. Phys. **13**, 1020 (2017).
[47] M. J. Kreder, D. Daniel, A. Tetreault, Z. Cao, B. Lemaire, J. V. I. Timonen, and J. Aizenberg, Phys. Rev. X **8**, 031053 (2018).
[48] M. R. Gunjan, A. Kumar, and R. Raj, Langmuir **37**, 6601 (2021).
[49] H. K. Khattak, S. Karpitschka, J. H. Snoeijer, and K. Dalnoki-Veress, Nat. Commun. **13**, 4436 (2022).
[50] P. S. H. Forsberg, C. Priest, M. Brinkmann, R. Sedev, and J. Ralston, Langmuir **26**, 860 (2010).
[51] T. Kajiya, A. Daerr, T. Narita, L. Royon, F. Lequeux, and L. Limat, Soft Matter **9**, 454 (2013).
[52] R. Lhermerout and K. Davitt, Soft Matter **14**, 8643 (2018).
[53] B. Roman and J. Bico, J. Phys. Condens. Matter **22**, 493101 (2010).
[54] Z. Cai and J. T. Pham, ACS Appl. Polym. Mater. **4**, 3013 (2022).
[55] A. Hourlier-Fargette, J. Dervaux, A. Antkowiak, and S. Neukirch, Langmuir **34**, 12244 (2018).
[56] A. Naga, A. Kaltbeitzel, W. S. Y. Wong, L. Hauer, H.-J. Butt, and D. Vollmer, Soft Matter **17**, 1746 (2021).
[57] R. W. Style and E. R. Dufresne, Soft Matter **8**, 7177 (2012).
[58] M. A. Biot, J. Appl. Phys. **12**, 155 (1941).
[59] Y. Hu, X. Zhao, J. J. Vlassak, and Z. Suo, Appl. Phys. Lett. **96**, 121904 (2010).
[60] J. D. Berman, M. Randeria, R. W. Style, Q. Xu, J. R. Nichols, A. J. Duncan, M. Loewenberg, E. R. Dufresne, and K. E. Jensen, Soft Matter **15**, 1327 (2019).
[61] M. M. Flapper, A. Pandey, S. Karpitschka, and J. H. Snoeijer, arXiv:2209.00887.
[62] Gelest Inc., Polydimethylsiloxane, Trimethylsiloxy Terminated, 5 Cst, https://www.gelest.com/product/DMS-T05/.
[63] D. W. McCall and C. M. Huggins, Appl. Phys. Lett. **7**, 153 (1965).
[64] K. Saalwächter and S. Seiffert, Soft Matter **14**, 1976 (2018).